Velocity Profile of the Ionized Disk and the Mass of the Black Hole in M87

Sandip K. Chakrabarti

Max-Planck-Institut für Astrophysik, Garching bei München,

Karl Schwarzschild Str. 2, D-85740 Germany

and

Theoretical Astrophysics, Tata Institute of Fundamental Research[1],

Homi Bhabha Road, Bombay 400005, India e-mail: chakraba@tifrvax.tifr.res.in

Received _____; accepted _____

[1]Permanent Address

ABSTRACT

We present a theoretical model for the ionized disk in M87 which includes spiral shock waves. The line emission profiles computed from this model at various positions on the disk are found to be in agreement with the recent Hubble Space Telescope results. Based on this model, we find that the ionized disk comprises two-armed giant spiral shock waves which extend from around 0.1 arc sec from the center to at least 1 arc second or more. Our model requires that the mass of the black hole be $(4 \pm 0.2) \times 10^9 M_\odot$ and the inclination angle to be $(42 \pm 2)^\circ$. We predict the nature of the line profiles at many other locations of the disk which could be verified in future observations.

Subject headings: accretion, accretion disks — galaxies: individual (M87) — galaxies: nuclei — line profiles — shock waves.

1. Introduction

Using the Faint Object Spectrograph (FOS) on Hubble Space Telescope (HST), Harms et al. (1994, hereafter H94) have recently reported the spectroscopy of central region of the elliptical galaxy M87. Ford et al. (1994, hereafter F94) using Wide Field Planetary Camera-2 have imaged the disk in H_α+[NII] and find an ionized disk with spiral structures of two (or more) arms. From the kinematical arguments, based on the Doppler shifts of several lines emitted from the disk, and assuming a Keplerian motion of the emitting gas, they conclude that the mass of the disk plus the nucleus: $M_c(R < 18\mathrm{pc}) = (2.4 \pm 0.7) \times 10^9 M_\odot$ and the inclination angle of the disk with the line of sight is $i = (42 \pm 5)^\circ$.

In the present paper, we provide a complete description of the velocity field of the ionized disk and compute shapes of typical line profiles expected from various regions of the disk. Our analysis is based on the solution of a non-axisymmetric disk model which includes two armed spiral density waves possibly observed in the HST data and therefore our disk model is intrinsically non-Keplerian. We find a very good agreement between the theoretical and observed line profiles as regards to the Doppler shifts, line widths and the intensity ratios. We generally confirm the conclusions of F94 and H94 regarding the mass of the black hole and the inclination of the disk although we believe that the mass of the central black hole is somewhat higher — close to $4 \times 10^9 M_\odot$. We interprete this to be due to the underestimation of the mass in previous reports which assume Keplerian motions of the emitting gas.

Based on the observed H_α flux and the electron density, F94 computes the mass of the ionized disk to be at most $10^4 M_\odot$ which is small compared with the central black hole. Assuming that the neutral disk mass to be of same order, it is unlikely that the observed spiral feature is due to the self-gravity of the disk. In a binary system with a thin accretion disk, the companion can induce two armed spiral shocks in the disk (e.g., Matsuda et al.

1987, Spruit 1987, Chakrabarti & Matsuda, 1992). In the case of active galaxies, a passing companion or even a globular cluster which is more massive than the disk can induce the same effect, but the spiral structure need not be stationary (Chakrabarti & Wiita 1993). The lifetime of the spiral structures may be of the order of a few Keplerian periods after which they break up and disappear at higher radius. It is possible that one such broken piece of the spiral shock structure may be visible in Fig. 3 of the M87 disk (F94). This figure indicates the existence of a third spiral arm which is presently no longer attached to the nucleus and is about half an arc second away. Because of this, we concentrate on disk solutions which include only two spirals. We have tested our solution with three arms as well but do not find satisfactory results to match with the observations.

The spiral shock wave solution is described in detail in the literature (Chakrabarti, 1990ab) and therefore it will not be presented here. The general procedure of obtaining the intensity of line emissions from such a disk is also presented elsewhere (Chakrabarti & Wiita, 1994) where it was shown that the time variability of the line emissions from the broad line radio galaxies such as ARP 102B and 3C390.3 can be understood well using non-Keplerian disk with spiral shock waves. In Section 2, we present the model assumptions. We also briefly discuss the analytical model and the procedure followed to obtain the disk line emission. In Section 3, we present the assumptions which went into fitting the observed line profiles in M87. In Section 4, we produce the parameters which yield the best fit and compare line profiles obtained from our disk model with those presented in H94. We also predict the nature of the profiles in regions not yet observed by HST. Finally, in Section 5, we present our conclusions.

2. Model Equations

Since we shall be discussing physical processes far away from the black hole, a Newtonian theory of the spiral shock wave in a quasi-three dimensional accretion disk will suffice. A general theory of such spiral shocks in the context of non-relativistic accretion disks is presented in Chakrabarti (1990a, hereafter Paper 1) and that including relativistic corrections is presented in Chakrabarti & Wiita (1994). In these works, for simplicity, the spiral structure is assumed to be self-similar, i.e., the angle subtended by the arms with the radial vector is assumed to be constant with radial coordinate.

In a self-similar disk, the velocity components vary as,

$$u' = x^{-1/2} q_1(\Psi), \quad v' = x^{-1/2} q_2(\Psi), \quad \text{and} \quad a' = x^{-1/2} q_3(\Psi), \tag{1}$$

where, u', v', and a' are the radial, azimuthal and sound velocities, respectively, $\Psi = \phi' + B\ \log(x) = constant$ defines the spiral coordinate, x is the radial co-ordinate r' in units of GM/c^2, M being the mass of the central black hole, and B =tan β, with β as the pitch angle of the spirals. The functional behaviors of $q_i(\Psi)$ are self-consistently determined from the two-and-a-half dimensional Euler equations: all the terms on the equatorial (r', ϕ') plane are kept, while the advective terms are dropped in the vertical direction and a hydrostatic equilibrium is assumed in that direction. The assumption of hydrostatic equilibrium may break down in the post shock region as the flow becomes hotter and expands in the transverse direction. However the gravitational influence of the central object is expected to extend about a distance of 300pc and unless the disk violently oscillates, the vertical velocity component is not expected to be high compared to the radial or azimuthal component. Therefore, the assumption of hydrostatic equilibrium is a good one to make under the circumstances. We assume the flow to obey an equation of state: $P = K(x,\ \Psi)\rho^{\gamma}$, where, P and ρ are pressure and density respectively, and $\gamma = 1 + 1/n$ is a constant, with n as the polytropic index. For an assumed number of shocks, given the pitch angle β, and any one of the velocity components on the sonic surface (we supply

q_{2c}), the entire set of equations can be solved for all the kinematic quantities $q_i(\Psi)$ as well as the polytropic index n of the disk. For our purpose in this paper, knowledge of these quantities are sufficient to obtain the velocity fields and line profiles. In a self-similar disk in hydrostatic equilibrium in the vertical direction, pressure, density and the entropy function K are found to vary as (Paper 1):

$$P = x^{-5/2} q_p(\Psi), \quad \rho = x^{-3/2} q_\rho(\Psi), \quad \text{and} \quad K = x^{\frac{3\gamma}{2}-\frac{5}{2}} \frac{q_p}{q_\rho^\gamma} \tag{2}$$

For a complete knowledge of the thermodynamic quatities, one has to supply another boundary condition, say q_ρ at a point. This, together with Eqn. (2) and the definition of the sound speed $a = (\gamma P/\rho)^{1/2}$, one can obtain all the necessary quantities. One important point to note is that since entropy must increase as the matter accretes (as x decreases), one must consider only those solutions which yield $\gamma < 5/3$, or $n > 3/2$. A few examples of the spiral shock solutions are given in Paper 1. For the sake of convenience q_3 as defined here is square root of q_3 of Paper 1. For comparison: in a strictly Keplerian flow, $q_2 = 1$ and $q_1 = 0$ identically everywhere. The sound speed in a Keplerian disk varies as $a \propto x^{-3/8}$, so q_3 cannot be compared directly with the Keplerian value.

The velocity components in above equations are transformed to the observers frame and relativistic corrections are made following Chen, Helpern & Fillipenko (1989, hereafter CHF) and Chakrabarti & Wiita (1994). We assume a power law emissivity,

$$\epsilon(x) \propto x^{-q}, \tag{3}$$

over the boundaries (x_{in} and x_{out}) of the line emitting region of the disk. The index q is expected to be within the range $1 \leq q \leq 3$ (e.g., Tylenda 1981; Smak 1981; CHF). The intensity of line emission at a given frequency is then obtained, following the approach of CHF, to be

$$I_\nu \propto \int_0^\infty \epsilon(x) \frac{D^3}{v_{th}} \exp[-\frac{1}{2}(\frac{\nu/D - 1}{v_{th}})^2] d\Omega, \tag{4}$$

where v_{th} characterizes the line broadening due to thermal motions of the emitting particles which we choose to be constant for simplicity. Here, $D = \nu/\nu_e$, is the Doppler factor with ν_e as the emitted frequency and ν as the observed frequency. The solid angle $d\Omega$ is given by $b\ db\ d\phi/d^2$, where b is the impact parameter of the photon (Chakrabarti & Wiita 1994; CHF) and d is the distance to the AGN. Instead of using constant v_{th}, one could also choose the thermal velocity, $v_{th} \propto (u^2 + v^2)^{1/2} h(x)/x = Q_{th} q_3 (q_1^2 + q_2^2)^{1/2} x^{-1/2}$, where $h(x) = x q_3$ is the local half-thickness of the disk and Q_{th} is a proportionality constant. The resulting line profiles with a suitable Q_{th} appear to be very similar as those with a constant v_{th}.

3. Fitting Procedure of the HST Results

For a given system, the general procedure of fitting the line profiles with the theoretical result would be to supply the following quantities: B and q_{2c} to obtain the velocity profiles in the disk, and the inclination angle i, the inner and outer edges of the emitting regions, x_{in} and x_{out} respectively, the emissivity law q, thermal broadening velocity v_{th} and the mass of the black hole M to obtain the line intensities. Among the seven positions of the disk pointed at by HST (see Fig. 1b of H94), we shall be interested in results obtained from the regions marked as positions 1, 2, 4, 5 and 6 since the emission line profiles are prominent in these regions. Figure 1 schematically shows these regions as dotted circles. Each of the circular apertures is of diameter 0.26 arc sec which corresponds to an absolute length of 18pc at the distance of M87 (assumed to be at 15Mpc). Since the absolute distances and the position angles of all the positions are provided, we do not require x_{in} and x_{out} for each of these regions separately– fixing a mass of the black hole provides the coordinates x and Ψ for each of these positions. For simplicity, while comparing results, we integrate the zone confined by the spiral coordinates surrounding a circular region. The successive (solid) circles are drawn with diameters of 0.26 arc sec, 0.78 arc sec and 1.3 arc sec respectively.

The regions I-VI are drawn at $\delta\Psi = 60^{\circ}$ intervals and the regions VII-XVIII are drawn at $\delta\Psi = 30^{\circ}$ intervals.

In Fig. 1, we also present schematically the spiral shock waves (thick curves) marked by Ψ_{s1} and Ψ_{s2} and the sonic surfaces marked by Ψ_{c1} and Ψ_{c2}. The direction of rotation is shown by an arrow. The line profiles calculated in regions marked from I to XVIII are presented in §4 as predictions of the model.

Observational results have been obtained by digitizing the line profiles from Figs. 1b and 2 of H94 and converting the observed wavelengths into wavelengths in the rest frame of the disk. First we fit the profiles of Position 4 (nucleus) and check if the same set of parameters consistently reproduces the profiles in Positions 1, 2, 5 and 6. Though different lines show different behaviors in the observations, a general trend is found to emerge which is the following: The line intensity from Position 4 is roughly 2 to 2.5 times stronger than that from Positions 5 and 6 and about 4 to 6 times stronger than that from Positions 1 and 2. The red shifted lines in Positions 5 and 6 are stronger than the blue-shifted components in some cases (e.g. [NII] at λ6584Å and [SII] at λ6731Å) but weaker at other cases (e.g., [O III] lines at $\lambda\lambda$4959Å and 5007Å). Since our model is for general line behavior, clearly, we cannot, for the same spiral structure, explain these unequal asymmetries in different lines without making further assumptions with respect to the inhomogeneities in the compositions, the variation of the emissivity exponent q and other physical processes such as photoionization, which are not included here. (In our model, intensity asymmetries can be different in different position angle of the shock.) We thus chose to ignore modeling the exact asymmetries in different line intensities, and concentrated on the basic features, such as the Doppler shift and the average behavior of the intensity ratio from one position to the other.

While fitting the line profile from the nuclear region (Position 4), we are faced with the

dilemma that whereas some lines clearly show splitting in the central region (e.g., [NII] at λ6584Å and H_β at λ4861Å) others do not (e.g., [OIII] at λ5007Å). The latter line widths however show indications of the split, as though they are superpositions of the splitted lines with possibly some additional components along the line of sight to smear out the valley. In our model, we do see the splitting in the nuclear region in some phases of the spirals. It is possible that different lines are excited at different regions of the spiral and therefore 'see' different phases.

Regarding the sensitivity of the emitted lines on the fitting parameters, we wish to mention that the emitted line profiles are found to be very sensitive to the relative phase of the spiral shocks with respect to the line of sight. Thus the spirals were first rotated around the axis (for each set of above mentioned parameters) and the results were found to be best fitted when the shocks were placed as the thick curves in Fig. 1 in relation to the observed positions. (The rotation by an angle ϕ_s is done with respect to a fiducial direction defined by $\phi' = \Psi = 0$ at $x = 1$.) Thus, we find that the results from Positions 5 and 6 may actually correspond to emissions from the hotter *post-shock* regions. As the flow crosses the shock at Ψ_{s1}, it becomes subsonic and hot, which produces the emissions in Position 6. The flow subsequently becomes supersonic at the sonic surface at Ψ_{c1} and passes through the shock at Ψ_{s2} producing the emission in Position 5. This becomes supersonic again at Ψ_{c2} and the cycle continues. Thus we believe that the spiral arms which are observed in the H_α+[NII] image (F94) actually represent post-shock dissipative regions.

4. Analytical Results and Comparison of Line Profiles

A two-armed spiral shock solution in a self-similar disk forms within a limited region of the parameter space spanned by the spiral angle β and the velocity coefficient q_2 at the sonic

surface. The velocity coefficients (q_is) as defined in Eqn. 1 remain constant on a given spiral curve but vary with Ψ and therefore, for a given x, on the azimuthal angle ϕ'. In Figure 2, we present the variation of q_{1-3} as functions of the spiral coordinate $\Psi = \phi + \tan\beta \log(x)$, for $\beta \sim 9^o$ and $q_{2c} = 0.54$. To obtain the actual velocity (in units of the velocity of light) at a given point on the disk, one simply has to divide these numbers by $x^{1/2}$, where x is in units of GM/c^2, half of the Schwarzschild radius. The curves are drawn from the post-shock region (left end) to the pre-shock (right end) in between two shock waves, as the flow passes through the sonic surface $\Psi = 0$. The sound speed coefficient (long-dashed) increases from 0.53 to 0.634 at the shock, a jump of about 20% which implies a jump of about 40% of the temperature at the shock front. The azimuthal velocity coefficient (short-dashed) jumps from 0.92 to 0.27 at the shock front, indicating a strong dissipation of angular momentum each time the flow passes the shock front (Paper 1). Notice that $q_2 < 1$ always, i.e., the flow is entirely sub-Keplerian. The radial velocity coefficient (solid) goes down from 0.46 to 0.36 at the shock front while becoming negative in some region. Thus the orbit is elliptical. The Mach number (defined with respect to the velocity component normal to the shock) jumps from 1.86 in the pre-shock flow to 0.51 in the post-shock flow, which signifies a jump by a factor of 3.67, i.e, the shock is relatively strong. Our procedure finds the polytropic index n self-consistently which in this case happens to be 2.02 and $\gamma \sim 1.5$. The angle between the sonic surface and the preceding shock is $\sim 120^\circ$, which corresponds to the locations $\Psi_{c1,c2}$ drawn in Fig. 1.

In the following discussion, we shall choose this solution. Before we present the comparison, we point out a simple but crucial result: the azimuthal velocity varies from 27% to about 92% of the Keplerian value with an average of roughly 60%. As a result, if the effects of radial motion on the line profiles are ignored, we should expect that the required mass of the black hole to be higher by a factor of $\sim 0.60^{-2} \sim 3$ to explain the same frequency shift. (This argument does not depend upon the inclination angle or emissivity

or the degree of thermal broadening.) As we show below, in reality, we require the central mass to be around $4 \times 10^9 M_\odot$, which is roughly twice as high. This is also an indication that the radial motions play an important role in shaping the line profiles.

Figure 3 shows the line profiles as obtained from the theory (solid) and the observations (dashed) made from various positions of the disk. The mass of the black hole is chosen to be $4 \times 10^9 M_\odot$ and the other parameters are: $i = 42^\circ$, $v_{th} = 0.0005$ and $q = 2.9$. The dot-dashed curve is the Position 4 observation of [NII] at λ6584Å (with H_α blended towards blue widening the base considerably) and the short-dashed curves are the Positions 4, 5, 6 observations of [O III] line at λ5007Å. The observations from Positions 1 and 2 roughly match (eye estimation was made since no detail line profiles were presented in F94 and H94) the solid curves drawn for the corresponding positions. We scaled vertically the observed [O III] line at Position 4 so that it may match the intensity of the theoretical profile. The scaling factor is then reduced by 35% to obtain the factor for the observed lines at Positions 5 and 6 which are plotted as well. We also scale separately the Position 4 observation of [N II] (dot-dashed curve) so as to superpose this plot. The [N II] lines at Positions 5 and 6 were heavily blended with H_α lines and were not plotted. But it was noted that these lines are red-shifted similarly as the theoretical solid curves at these locations.

The general agreement of the observed line profiles and the theoretical curves show that the mass of the black hole is possibly much higher than the previously computed values. One important point to note is that the line width of the wing for the Position 4 observation can be matched with the theoretical profile only if the inner edge of the spiral shock be chosen to be at around $x_{in} = 2 \times 10^4$ (i.e., ten thousand Schwarzschild radii). We find that for x_{in} less than this value the width of the lines at the wing becomes very broad. Since temperature $T \propto x^{-1}$ in our model, it increases by at least a factor of 10 along curve of constant Ψ, as one moves in from 1 arc sec to 0.1 arc sec distance from the center. Thus,

either the shocks do not extend below this radius, or, if they do, they become so hot that line emission properties change dramatically.

We see above that the constraints from the wing width indicate $M(R < x_{in}) \sim 4{\times}10^9 M_\odot$ which is a more stringent limit on the central mass than previously presented. It could be easily shown that the results do not match with observations if the mass of the black hole is chosen very much differently. If the black hole is chosen to be lighter, the line shifts are found to be much less than the observed values. Similarly, with a higher mass, the line shifts are found to be higher. Based on the nature of the fit, we believe that the mass of the black hole and the inclination angle could be within the range $M = 4.0 \pm 0.2 M_\odot$ and $i = 42 \pm 2^\circ$ respectively. Thus the mass estimate from our calculation is accurate to a few percent. This is to be contrasted with the mass estimate of H94, where $\pm 30\%$ error bar in the mass is obtained by forcing the flow to have Keplerian velocity.

In Figures 4(a-b) we present the predictions of the line profile from the theoretical model with the same parameters. In Fig. 4a, lines from regions marked I-VI and in Fig. 4b, lines from the regions marked VII-XVIII are presented. Because of the non-axisymmetric nature of the flow, the line intensities and the frequency shifts do not vary monotonically. Future observations from these regions with similar aperture can be used to verify such a flow behavior in the disk.

In anticipation of observations with 0.09 arc sec aperture, we present in Figure 5 the predicted behavior of the line profile closer to the center. We chose regions (a-f) with diameter 0.09 arc sec, centered at 0.135 arc sec, and with position angles 81°, 144°, 201°, 261°, 321° and 21° respectively. These positions are radially below positions I to VI of Fig. 1.

5. Concluding Remarks

We have modeled the ionized disk in M87 assuming that the disk has two stationary spiral shock waves. The line profiles computed from this model generally agree with those recently observed by Hubble Space Telescope (F94, H94) provided the mass of the central black hole is about $4 \times 10^9 M_\odot$. Mass evaluated from our model is higher compared to the previously estimated values. This is primarily due to the fact that the azimuthal velocities in disks with shock waves are sub-Keplerian and therefore one requires a higher central mass for the same frequency shift. Our analysis, however, agrees with the estimated inclination angle $i \sim 42^\circ$. Another significant observation is that the spiral arms which are observed in H_α+ [NII] images (H94, F94) may actually correspond the post-shock emission regions in the theoretical model where the observations 5 and 6 (H94, F94) were made. We also make prediction of the variation in line shapes from different positions in the disk, and thus our model can be tested by future observations. If this sub-Keplerian disk model is correct, it may generally indicate that so far, the masses of the galactic nuclei are seriously under estimated. This may have other ramifications, such as the constraint on the the dark matter candidates in galaxies and in the universe in general. Also, the existence of such a super-massive black hole at the galactic nucleus may indicate that since the time of catastrophic formation of the black hole during the proto-galactic phase, the central mass may have significantly increased through accretion of gas and tidal capture of stars.

Though we have advanced the model of line emission from shock heating, it is possible that some degree of photoionization may not be ruled out. One way to distinguish different emitting region is to study the intensity ratios of different lines (Veilleux & Osterbrock, 1987). From the HST data (H94), this ratio is found to vary from position to position. Generally, the ratios are: $([N\ II]\lambda6583)/(H_\alpha\ \lambda6563) \sim 3.0$, $([O\ III]\lambda5007)/(H_\beta\ \lambda4861) \sim 1.5\ -\ 2.2$, $([S\ II]\lambda6716 + \lambda6731)/(H_\alpha\ \lambda6563) \sim 0.9\ -\ 1.0$,

$([O\ I]\lambda6300)/(H_\alpha\ \lambda6563) \sim 0.5$. These ratios definitely lie in the AGN region and not in H II region (see Figs. 4-6 of Veilleux & Osterbrock, 1987). Whereas the plot of $OIII/H_\beta$ vs. SII/H_α falls close to the shock heating curve of Shull & McKee (1979), other plots fall on the right of it and could possibly be fitted with photoionization models (e.g., Ferland & Netzer, 1983; Stasinska 1984) as well. Infact, the situation is similar to the case of LINERs where it is difficult to distinguish the origin from the ratio alone. One the one hand, Keplerian disks would be very cold at distances of 10^5 Schwarzschild radius to emit the observed lines. On the other hand, if the flow is really transonic as in our model, one draws an unavoidable conclusion that the sound velocity is several hundred Km s^{-1} at this distance, and therefore the tempereture in equatorial plane is $\sim 10^7$K! Thus, the disk is probably a mixture of ionized and neutral components with only a fraction of matter participating in the process of shock formation.

We have already mentioned that the vertical equilibrium model may breakdown in the post-shock region where some vertical motion is expected after the flow thickens at the shock. In the present case, the shock thickness ($\propto q_3$) is expected to be higher by only 20% from that of the immediate pre-shock flow. In reality, in presence of viscosity and the resulting smearing effects this velocity need not be high. Furthermore, the ratio $h/x = q_3 = 0.64 < 1$ in the post-shock region so that our treatment is probably justified. A corollary of the thickening of the disk at the shock is the shadowing effect which is expected to obscure the pre-shock disk. However, we have ignored this effect for two reasons: (a) the shock is almost straight and is located only a few degrees away from the projected line of sight on the disk plane and (b) the positions 5 and 6 fall in the post-shock region, while the positions 1 and 2 are far away from it and therefore free from shadowing effects. If the shadowing effect is important (namely, if the thickening is not gradual but abrupt), the resulting line profile, emitted from regions IV & XIII would have intensity a few (≤ 5) percent smaller than what is predicted in Figs. 4(a-b). We notice from the H_α+[NII] image

(F94) of the spiral arms extended beyond 1 arc sec that the spiral waves definitely are not self-similar. They suddenly bend by a higher angle. However, within about 1 arc sec, they are roughly straight and thus may actually correspond to the post-shock regions of the $\beta \sim 9^{\circ}$ shocks which we model here. We also conclude that the properties of the shock and/or the emission property of the disk must be different very close to the nucleus, since extension of the shocks below 10^4 Schwarzschild radius causes the line widths to be unduly higher and the theoretical results deviate from observations considerably.

The author is grateful to H. Ford and A. Kochhar for allowing him to have copies of their papers (F94 and H94) before publication. He thanks P. Schneider for carefully reading the manuscript and F. Mayer and M. Camenzind for helpful comments. The author is also thankful to the Indian National Science Academy and Deutsche Forschungsgemeinschaft which made his visit to the Max Planck Institute possible.

REFERENCES

Chakrabarti, S.K. 1990a, ApJ 362, 406 (Paper 1)

Chakrabarti, S.K. 1990b, Theory of Transonic Astrophysical Flows, (Singapore: World Scientific)

Chakrabarti, S.K. & Matsuda, T. 1992, ApJ, 390, 639

Chakrabarti, S.K., & Wiita, P.J. 1993, ApJ, 411, 602

Chakrabarti, S.K., & Wiita, P.J. 1994 ApJ, (in press)

Chen, K., Halpern, J.P., & Fillipenko, A. 1989, ApJ, 339, 742 (CHF)

Ferland, G.J. & Netzer, H. 1983, ApJ, 264, 105

Ford, H.C., Harms, R.J., Tsvetanov, Z.I., Hartig, G.F., Dressel, L.L., Kriss, G.A., Davidsen, A.F., Bohlin, R., & Margon, B. 1994, ApJ Letters, (in press)

Harms, R.J., Ford, H.C., Tsvetanov, Z.I., Hartig, G.F., Dressel, L.L., Bohlin, R., Kriss, G.A., Davidsen, A.F., Margon, B. & Kochhar, A. 1994, ApJ Letters, (in press)

Matsuda, T., Inoue, M., Sawada, K., Shima, E., and Wakamatsu, K. 1987, MNRAS, 229, 295

Shull, J.M. & McKee, C.J. 1979, ApJ, 227, 131

Smak, J. 1981, Acta Astron. 31, 25

Spruit, H.C. 1987, A & A, 184, 173

Stasinska, G. 1984, A & A, 135, 341

Tylenda, R. 1981, Acta Astron. 31, 127

Veilleux, S. & Osterbrock, D.E. 1987, ApJ Supp. Ser., 63, 295

This manuscript was prepared with the AAS LaTeX macros v3.0.

FIGURE CAPTIONS

Fig.1: Positions (1, 2, 4, 5, 6) of the observed region of the disk, locations of the shock waves ($\Psi_{s1,s2}$) and sonic surfaces ($\Psi_{c1,c2}$). Also shown are regions I-XVIII. Predicted line profiles from these regions are presented in Figs. 4(a-b)

Fig. 2: Variations of the radial (solid), azimuthal (short-dashed) and sound (long-dashed) velocity coefficients q_i as functions of the spiral coordinate Ψ from the post-shock region (left end) to the pre-shock region (right end). $\Psi = 0$ represents the sonic surface.

Fig. 3: A comparison of the model (solid curves) and observed (dot-dashed for [NII] λ6584Å and short-dashed for [O III] λ5007Å) line profiles plotted against frequency. The model parameters are: $M = 4 \times 10^9 M_\odot$, $\beta = 9.1^\circ$, $q_{2c} = 0.54$, $q = 2.9$, $i = 42.0^\circ$, $v_{th} = 0.0005$. Model curves are marked with Position numbers on the disk (see Fig. 1)

Fig. 4(a-b): Predicted line profiles from the regions (a) I-VI and (b) VII-XVIII. See Fig. 1 for definitions of these regions.

Fig. 5: Predicted line profiles of regions centered at 0.135 arc sec and 0.09 arc sec diameter. The position angles of the profiles (a-f) are 81°, 144°, 201°, 261°, 321° and 21° respectively.

This figure "fig1-1.png" is available in "png" format from:

http://arXiv.org/ps/astro-ph/9411042v1

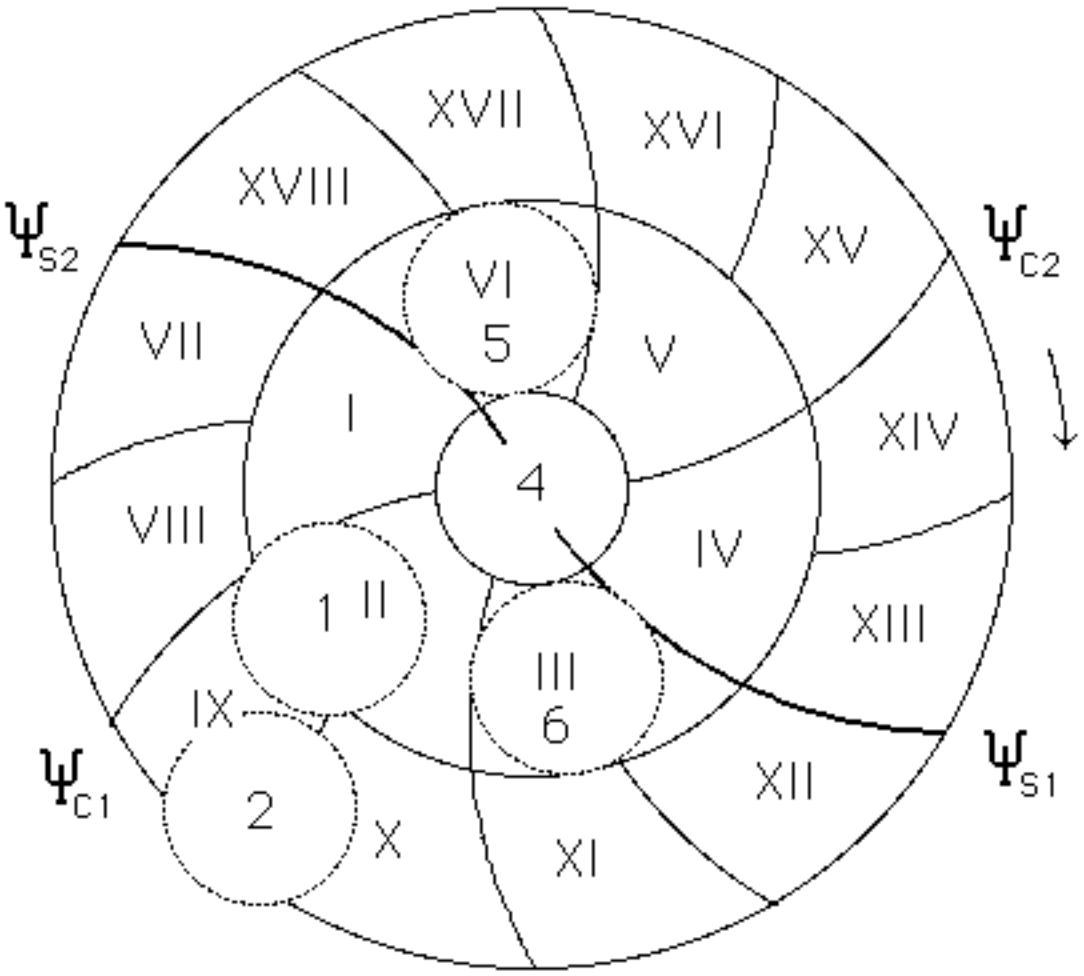
Ψ_{S2}
Ψ_{C2}
Ψ_{C1}
Ψ_{S1}
XVII
XVI
XVIII
XV
VI
5
VII
V
I
XIV
4
VIII
IV
1
II
XIII
III
6
IX
2
X
XII
XI

This figure "fig2-1.png" is available in "png" format from:

http://arXiv.org/ps/astro-ph/9411042v1

This figure "fig2-2.png" is available in "png" format from:

http://arXiv.org/ps/astro-ph/9411042v1

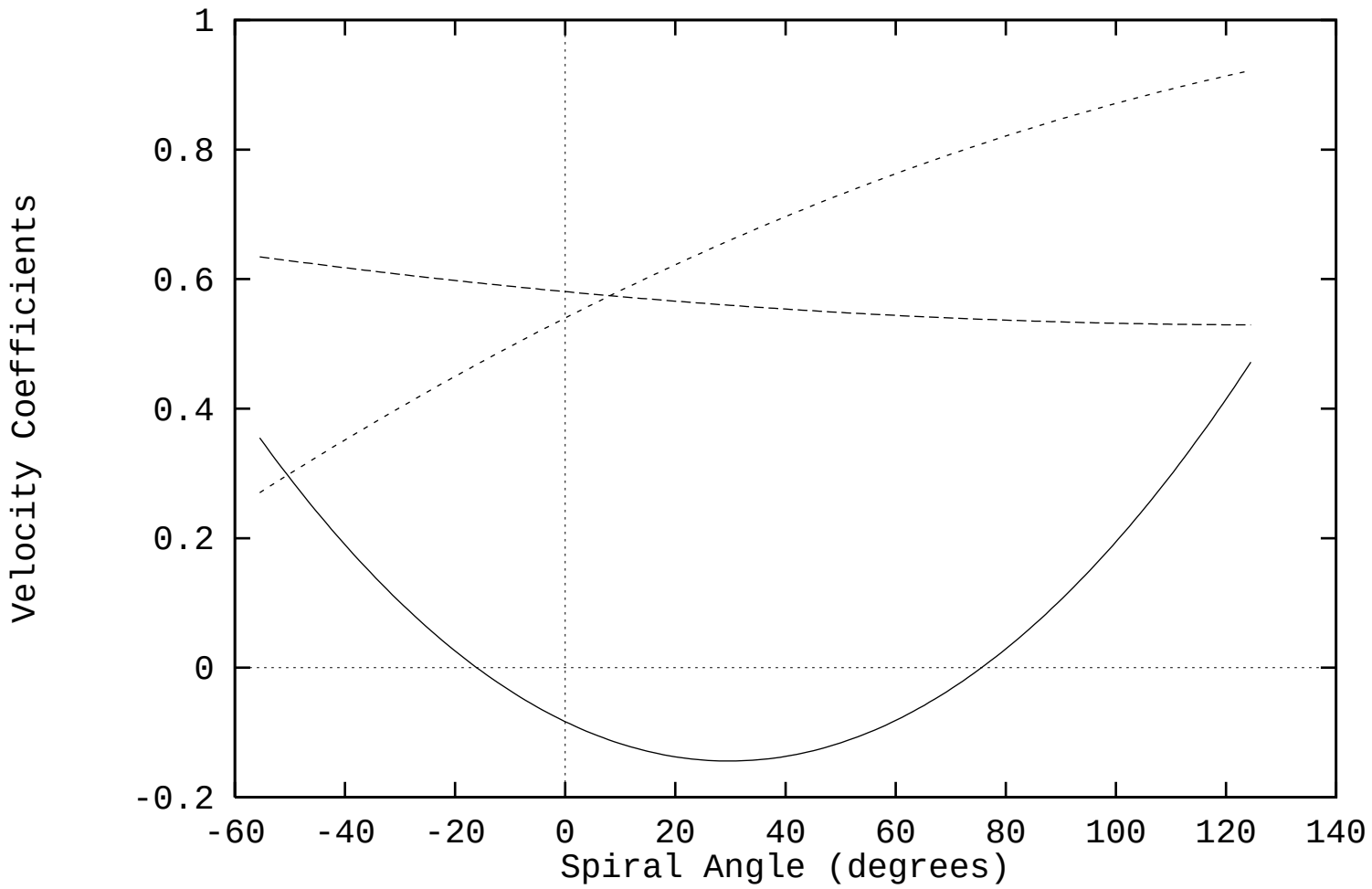
Velocity Coefficients
1
0.8
0.6
0.4
0.2
0
-0.2
-60
-40
-20
0
20
40
60
80
100
120
140
Spiral Angle (degrees)

This figure "fig2-3.png" is available in "png" format from:

http://arXiv.org/ps/astro-ph/9411042v1

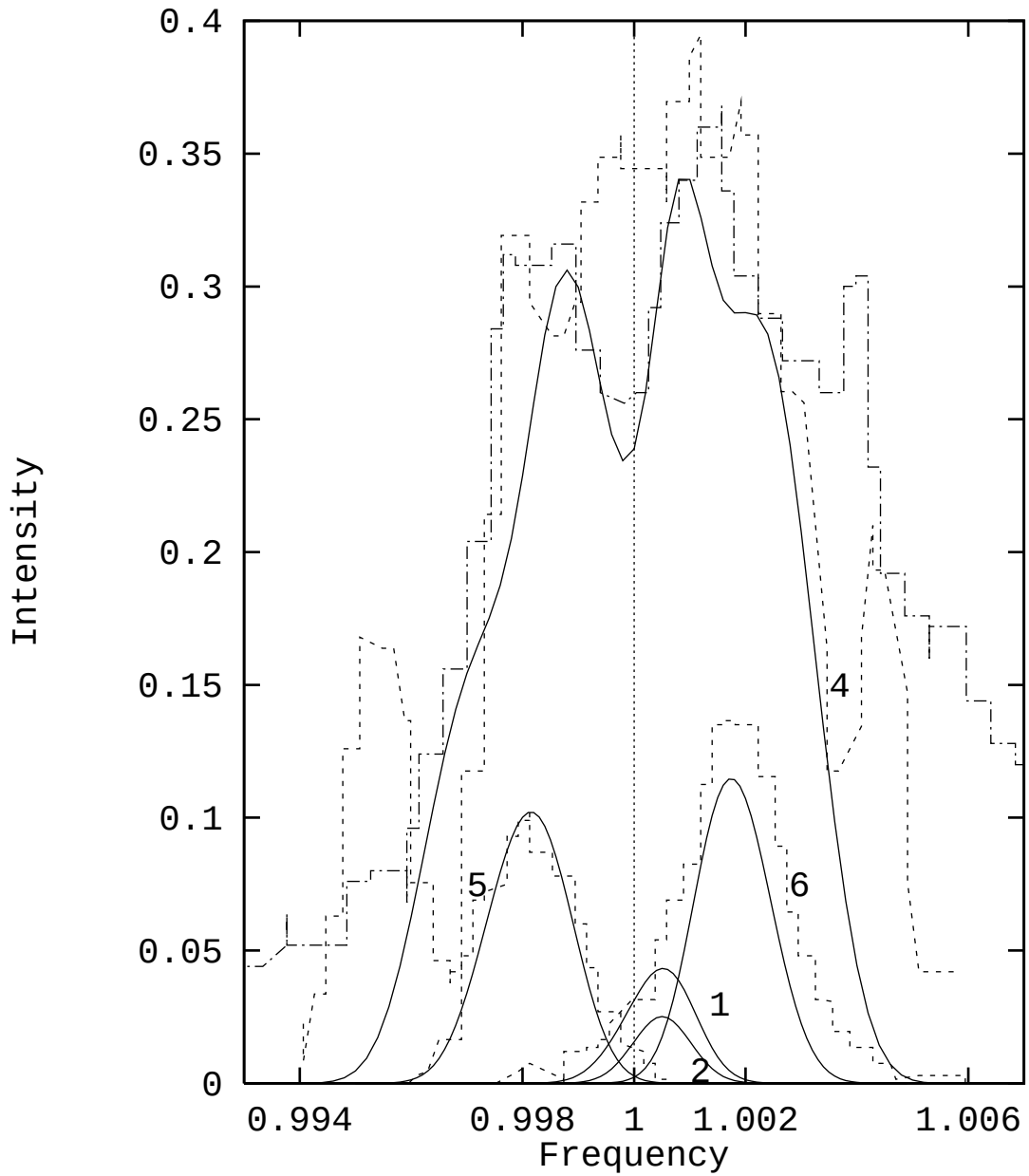
0.4
0.35
0.3
0.25
0.2
0.15
0.1
0.05
0
Intensity
0.994
0.998
1
1.002
1.006
Frequency
1
2
4
5
6

This figure "fig2-4.png" is available in "png" format from:

http://arXiv.org/ps/astro-ph/9411042v1

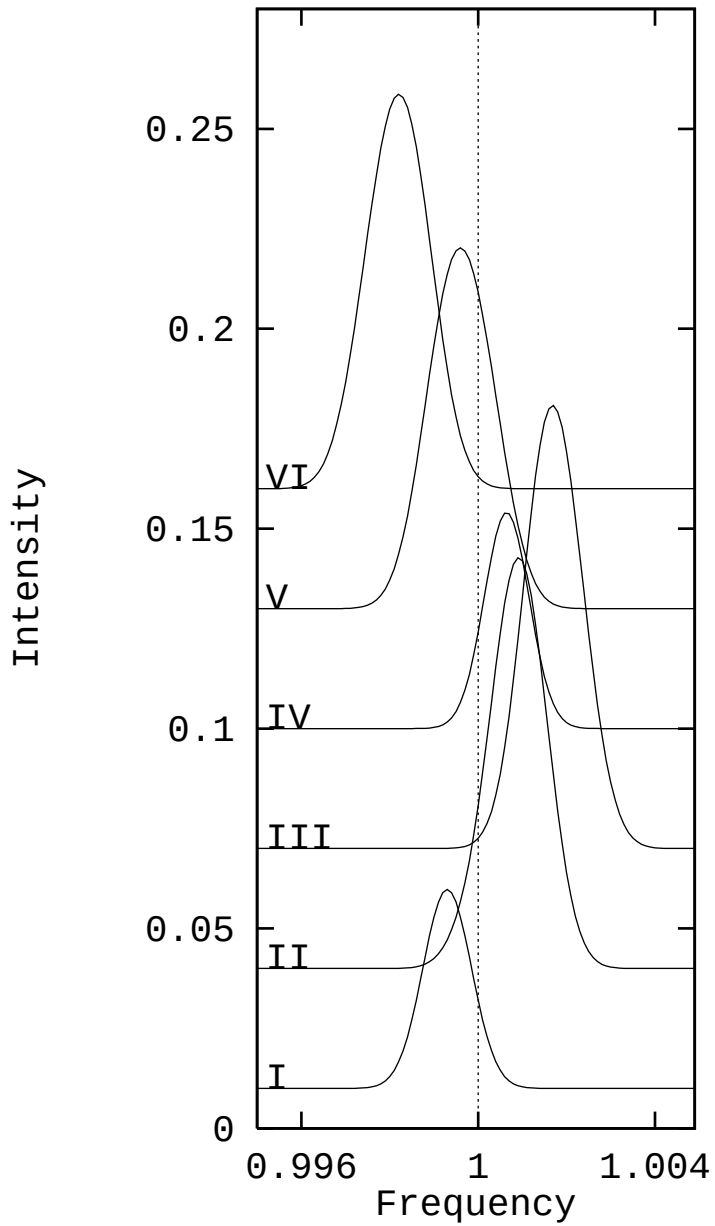
Intensity
0.25
0.2
0.15
0.1
0.05
0
VI
V
IV
III
II
I
0.996
1
1.004
Frequency

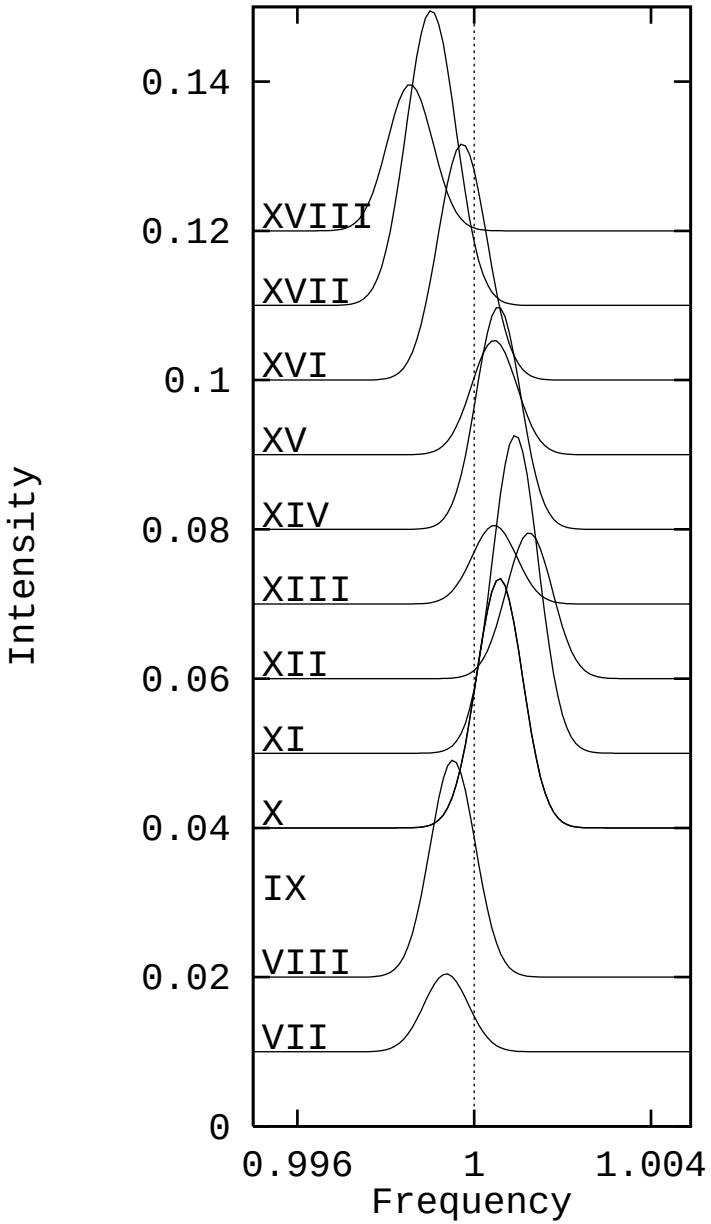
Intensity
0.14
0.12
0.1
0.08
0.06
0.04
0.02
0
XVIII
XVII
XVI
XV
XIV
XIII
XII
XI
X
IX
VIII
VII
0.996
1
1.004
Frequency

This figure "fig2-5.png" is available in "png" format from:

http://arXiv.org/ps/astro-ph/9411042v1

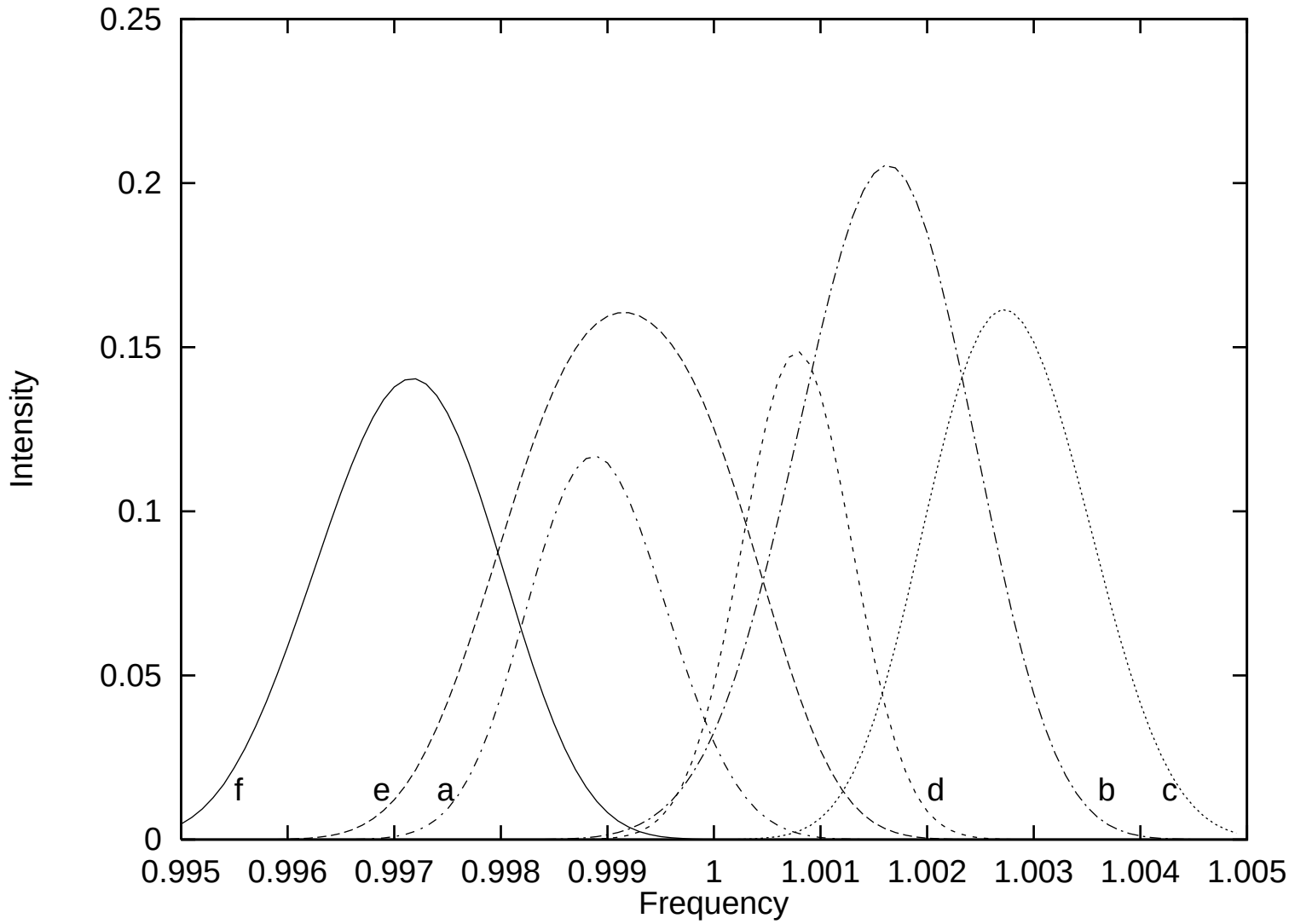
0.25
0.2
0.15
0.1
0.05
0
Intensity
0.995
0.996
0.997
0.998
0.999
1
1.001
1.002
1.003
1.004
1.005
Frequency
f
e
a
d
b
c